PROCESSING OF TiO_2/ TiC_xO_{1-x} NANO-CERAMIC COMPOSITE SEMICONDUCTOR: NOVEL RESULTS

S.SRIVASTAVA*

AMAN J. SHUKLA**

Abstract:

In this work, we present experimental studies for the processing of TiO_2/ TiC_xO_{1-x} Nanoceramic Composite. This paper reports the synthesis of TiO_2/ TiC_xO_{1-x} composite with Ti/C ratio 50:30 via spark plasma sintering route (SPS). The sinterability, microstructure and mechanical properties of the SPS processed sample was optimized with considering time and temperature. TiC_xO_{1-x} was reinforced in the TiO_2 matrix by the solid state reaction with TiO_2 and graphite. Different product was obtained by the carbothermal reaction at the different temperature. Fully dense composite with nano TiC_xO_{1-x} reinforcement was obtained after SPS at the high temperature. Fully dense composite shows superior hardness and toughness synthesis with SPS processes. Significant change in thermal conductivity is observed in these composite materials by the formation of different reinforcing constituent at the different temperature. These results suggest that the interface conditions strongly influence the thermal conductivity of the composite materials. Seeback studied was carried out for analyzing the nature of the composite materials. With the variation of temperature different types of the reinforcing constituents are formed with different charge carrier.

Key words: Nano-ceramic, SPS, hardness, thermal conductivity, Seeback coefficient

* Materials Science & Metallurgical Engineering, Maulana Azad National Institute of Technology, Bhopal-462051.

** Research & Technology Development Centre, Sharda University, G. Noida U.P.(India)-201306.

Introduction:

The spark plasma sintering technique is effective for any powder material application, but interest is especially high for nanocrystalline structures [1]. Generally, superfine materials have more surface area per unit volume than the same material made with larger particles. This, along with the way particles interact once compacted, "amplifies" material characteristics. One of the major challenges in the development of nanostructured/ultrafine non-oxide ceramics is the synthesis of non-agglomerated nanosized ceramic powders. One of the major challenges in the research on bulk nanoceramic composites is the synthesis of nanosized ceramic powders. Bulk nano-materials, having grain sizes typically smaller than 100 nm, possess appealing mechanical, physical, and tribological properties [2-6]. In theory, high-strength materials show an increase in strength, highly wear-resistant materials show higher wear resistance, highly magnetic materials show higher magnetism, and so on. Suitable applications include advanced lightweight armament, guidance optics and ultra-high-strength tooling. Nanostructured ceramics, metals and composites offer superior or a typical properties (non-linear optical, electric and magnetic characteristics, inverse Hall-Petch effect) comparing to classic counterparts [7, 8]. One of the key problems in nanotechnology is production of bulk nanomaterials because of thermal instability of nanocrystals which leads to a spontaneous grain growth. However, since SPS technology can sinter nanocrystalline material with very little grain growth and negative particulate effect, the door is now open to test and study new ideas in powder material applications. SPS technology can sinter materials without the use of binders. Most conventional powdered material sintering technologies require pre-forming and binders, and in many cases, expensive binder removal processes [9]. Binders weaken the part due to their susceptibility to chemical wear, reduced hardness and strength, and oxidation breakdown [10]. The availability of binder-less material could be valuable in numerous applications, including cobalt-less tungsten carbide, high-purity ceramic fuel cells and ceramic optics. In this research work, we focus the major work to develop TiO_2/ TiC_xO_{1-x} semiconducting composite materials via SPS technique.

Experimental procedure

Prior to carbothermal reduction, we prepared a nano rutile powder from chemical reaction technique. In the synthesis of TiO_2 particle, Titanium tetra isopropoxide was used as precursor and was mixed with HCl, ethanol and deionized water mixture, stirred for half an hour, in pH range of 1.5. 10 ml of deionized water was added to the above mixture and stirred for 2hours at room temperature. Finally the solution was dried at room temperature and the powder was annealed at 120^{o}C for 1 hour. The dried powder was mixed with gaphite and acetone in a high-density polyethylene jar. The planetary ball mill was used as grinding media. Mixed powders of TiO_2 and C material were mechanically alloyed in a planetary ball mill at ambient temperature. The powders (5 g) were mixed and sealed in a stainless steel vial (500 ml capacity) under an argon atmosphere. The mass ratio of ball to powders was 50∶1. Two kinds of hardened steel balls of φ 20mm and φ 6mm diameter were selected. The rotational speed was 200r·min^{-1}.TiO_2 and graphite mixture powders were ball-milled in a Ti/C atomic ratio of 50∶30. The mixed powder was milled for 4h (A) and 12 h (B).

The dry black powder mixture was sintered in an SPS apparatus in which the cylindrical samples are 10mm diameter and about 8nm in height at varying temperature. The dried powder mixture is sintered inside the SPS Chamber under a vacuum of 50-60 mtorr at different temperatures in the range of 1100-1500°C with a pressure of 30 MPa. The heating to sintering temperature is accomplished in 2 minutes. This resulted in a high heating rate of the order of 550-650 K/min. The final thickness of the sintered pressed discs was about 2-5 mm. The density of specimen was measured in ethanol, according to the Archimedes method. The hardness of the sintered discs was measured using the Vickers hardness test (VHN) at a load of 10 kg. Micro-structural investigation of the polished was performed using SEM and phase analysis by XRD. A schematic representation of a heater block–sink assembly with the sample is depicted in Figure. 1. It is a steady-state method where temperature differences between the source and sink are measured as a function of time and the sample holder and sample act as two parallel heat conducting paths. It is a steady-state method where temperature differences between the source and sink are measured as a function of time and the sample holder and sample act as two parallel heat conducting paths. First, the characteristics of the sample holder are measured, which determines the baseline or background thermal conduction and losses associated with the sample

stage. The second step consists of attaching the sample and measuring the new characteristics of the assembly. By subtraction of the background thermal conduction, the thermal conductivity of the sample is calculated.

Result and Discussion

The different types of non-stoichiometric TiC_x are formed by the carbo-thermal reduction of TiO_2 and C. The mixture was sintered at the different temperature through SPS process. Non stoichiometric reactions were utilized to synthesize the TiC_x in TiO_2 matrix. The formation of phase from the carbothermal reaction by SPS process was studied in temperature range of 1100 °C−1550 °C. The sample is absorbed the heat from the surrounding environment of the furnace, carried out the solid state reaction. The major interest in this process, when the sintering parameters have been mastered, is linked to the extreme rapidity of the thermal treatment. Thus, the consolidation time is greatly decreased from hours, in the case of the conventional sintering, too few minutes for the SPS process. Moreover, the sintering temperature can be diminished by a few hundred degrees compared to conventional sintering (Figure. 2) [10]. In short, SPS constitutes an innovative technique in the field of materials sintering and three distinguishing factors contribute to its enhanced densification compared to conventional sintering processes: i) dc current influence, ii) high heating rates, and, iii) the simultaneous application of pressure.

Figure 2 shows the variation of shrinkage (mm) with temperature. The study shows that the parameter controlling at the first order the sintering temperature range is the initial grinding of the powder. Following the linear shrinkage curves versus temperature, the shrinkage starts at 700^{o}C in both the powder. Difference in the shrinkage of both the sample appears at 800^{o}C, when as expected, the specific area of different powders starts to play the main role in the sintering mechanism under SPS conditions and a smaller grain size contribute to shifting the sintering towards “the low temperature” domain. It is also evident from the figure 2 that only slight change in shrinkage occurs in both the sample. This is due to nature of the compacted particles. During the SPS process, heat is concentrated primarily on the surfaces of the particles. Particle growth is limited due to the speed of the process and the fact that only the surface temperature of the particles rises rapidly. The entire process—from powder to finished bulk sample—is completed quickly, with high uniformity and without changing the particles’

characteristics. SPS technology is capable of achieving nearly 100% theoretical density in almost any metallurgical or ceramic material, including composites. By accurately controlling compression and temperature, SPS technology can control material porosity while maintaining strong particle bonds throughout the shape. TiO_2 and graphite mixture was compressed and achieved approximate 90% relative density. The variation of density of samples as a function of the sintering temperature is shown in Figure 3. The density of both the sample using mixture sintered at 1000^oC for 2min is 3.68 & 3.78g/cm^3 (91.2% of theoretical density of the mixture), and increases to 4.88g/cm^3 (98.2% of theoretical density of stoichiometric TiC) when the sintering temperature reaches 1500^oC. At this temperature TiO_2 tries to converts stoichiometric TiC.. From TiO_2 to TiC conversion in between different types of non-stoichiometric TiC_x are formed. At 1500^oC maximum TiC is formed with little amount of non-stoichiometric TiC_x. The relative amount of TiC_xO_{1-x} /TiO_2 varies by changing the temperature from 900 to 1550^oC. Relative density increases with temperature when a change in densification mechanism is noticed at 1100^oC-1500^oC. At the lower temperatures, densification is due to grain boundary diffusion which changes to plastic yield at higher temperatures. The change is due to a decrease in yield stress below the aforementioned temperature.

The grain shape size is similar to all temperature. The largest amount of grain has sizes of 50μ. SPS technology can produce true seamless bonding (dry and liquid phase bonding). Because the SPS process draws particles together and offers the ability to reach nearly 100% theoretical densities, the process can produce bonded parts that have no seam. Figure 4 shows the SEM microgarph of TiO_2 nanoparticles prepared by chemical precipitation route. The pure TiO_2 particles exhibited irregular morphology due to the agglomeration of primary particles and with an average diameter of 40-45nm.

Nanoparticles of TiO_2 was properly mixed with graphite powder and sintered in SPS furnace. From the sintering process, different type of the non-stoichiometric chemical reaction occurs between the TiO_2 and graphite. Figure 5 shows the SEM micro graph of the nanocomposite of TiC_xO_{1-x} embedded in TiO_2 matrix, sintered at the different temperature. Fine particles of TiC_xO_{1-x} were formed at the low temperature, and it was uniformly distributed in the TiO_2 matrix as shown in Figure 5a. As with increase temperature from 1100 to 1550^oC, the maximum amount of TiO_2 tries to convert into TiC. At the higher temperature, non-stoichiometric TiC_xO_{1-x} starts to agglomerate and try to convert stoichiometric TiC_x as shown in

Figure 5 b to c. This figure clearly reveals the presence TiC_xO_{1-x} embedded in TiO_2 matrix. Figure 4d shows SEM microgarph of TiC formed at the higher temperature. TiC formed at the higher temperature shows the irregular morphology due to the agglomeration of primary particles of non- stoichiometric TiC_xO_{1-x}. But the tendency of agglomeration of primary particles of non-stoichiometric TiC_xO_{1-x} has been reduced with increase the temperature from 1300 to 1500^oC. At the higher temperature graphite diffuses much faster and reacts with rest amount of TiO_2 and non- stoichiometric TiC_x. We can see that the morphology of the surface of TiC block is homogeneous and loose agglomeration. It can be seen from Figure.5 (a) and (d) that among TiC crystal grains lots of gas porosities distribute, which are caused by discharged gas CO in carbothermal reduction process. Figure 6 (a) and (b) shows XRD patterns of products prepared at 1100, 1200, 1300, 1400, 1500 and 1550 °C for 2 min when the molar ratio of TiO_2 to C is 4:1. This XRD graph represents the schematic view for the reduction of TiO_2 to TiC. The different intermediate phases are formed during the synthesis of TiC_xO_{1-x}. It can be seen that Ti_3O_5 phase and Magneli phase (Ti_4O_7) appear at 1100 °C. At 1200 °C, a large amount of Ti_2O_3 phases form while the peak intensity of Ti_3O_5 diminishes and Ti_4O_7 disappears. In fact, carbothermal reduction reaction of TiO_2 is a continuous process. Based on XRD results in Figure 6 and reaction thermodynamics between TiO_2 and C, the main reactions are:

$$nTiO_2+C=Ti_nO_{2n-1}+CO(n>4) \quad (1)$$

$$4Ti_nO_{2n-1}+(n-4)\,C=nTi_4O_7+(n-4)CO\ (n>4) \quad (2)$$

$$3Ti_4O_7+C=4Ti_3O_5+CO \quad (3)$$

$$2Ti_3O_5+C=3Ti_2O_3+CO \quad (4)$$

$$Ti_2O_3+(1+4x)C=2TiC_xO_{1-x}+(1+2x)CO \quad (5)$$

$$TiC_xO_{1-x}+(2-2x)C=TiC+(1-x)CO \quad (6)$$

At the same time, trace amount of solid solution TiC_xO_{1-x} is formed easily from TiC and TiO because their lattice parameters are approximately the same. At 1300 °C, TiC phase appears and the peak intensities of solid solution TiC_xO_{1-x} increase when the peaks of Ti_2O_3 diminish and Ti_3O_5 disappears, which indicates that TiC_x phase may form from TiC_xO_{1-x} with further reduction. At 1400 °C and 1 500 °C, Ti_2O_3 peak intensities diminish gradually and TiC_xO_{1-x} disappear while TiC peak intensities increase. At 1550 °C, only TiC phase is formed. The results

illustrate that the formation sequence of the products in vacuum should be Magneli phase (Ti_4O_7), Ti_3O_5, Ti_2O_3, TiC_xO_{1-x} and TiC. From the XRD analysis it implies that Ti_2O_3 is the lowest oxide phase before forming TiC_xO_{1-x} and TiC when carbon content in raw materials is enough.The finer the stoichiometric TiC powder particles, the higher the mechanical strength of the consolidated materials obtained. So it is necessary to calculate the lattice parameter for defining the stoichiometry of TiC powders by means of extrapolation technique [12-15] with the following equation:

$$a = a_o + a_o K \frac{1}{2}\left(\frac{\cos^2\theta}{\sin\theta} + \frac{\cos^2\theta}{\theta}\right) = a_o + K'' F(\theta) \tag{7}$$

$$a = d_{(hkl)}(h^2 + k^2 + l^2)^{1/2} \tag{8}$$

Where θ is the diffraction angle, a is the lattice parameter which could be determined by Eq.(7). a_0 is the true lattice parameter of TiC which could be determined by Eq.(8). In accordance with XRD patterns, we can draw the figure of lattice parameter versus Nelson-Riley function $F(\theta)$ and extrapolate to a_0 as θ=90°. Vickers hardness and indentation fracture toughness of TiC- TiO_2 is plotted against sintering temperature in Figure7. While the hardness of TiC- TiO_2 increases significantly with SPS-temperature, the indentation toughness data show little variation around 6-7.8 MPa $m^{1/2}$. The finer microstructure of the synthesized product in particular, the reinforcement of TiC in TiO_2 matrix is considered to play a major role in achieving high hardness. The composite materials achieve higher hardness at the higher temperature. At this temperature TiC_x/TiO_2 are tried to convert into TiC.

Under steady-state conditions the **K** of a material is defined as

$$K = \frac{Q_s'}{A}\frac{\Delta T}{\Delta L} \tag{9}$$

Where Q_S' is the amount of heat passing per unit time through a cross-section area A, and causing a temperature difference, ΔT, over a distance ΔL. QS' /A is therefore the heat flux that is causing the temperature gradient, $\Delta T/\Delta L$. The measurement of thermal conductivity therefore involves the measurement of the heat flux and temperature difference.

Thermal conductivity was also measured as a function of temperature for TiO_2/ TiC_xO_{1-x} Nano-composite as shown in Figure 8. TiO_2/ TiC_xO_{1-x} Nano- Composite have a very high thermal conductivity and the applicability of this technique for measurement of low K materials is demonstrated. It can be seen from Figure 7 that the thermal conductivity initially increases with increase the temperature due to formation of TiC_xO_{1-x} semiconducting materials. With increase the temperature graphite diffuse much faster and give the solid state reaction and form maximum amount of TiC_xO_{1-x} semiconducting materials. But this semiconducting compound reduces to TiC at the higher temperature. Therefore conductivity decreases with increase the temperature.

For measuring the Seebeck coefficient (S), the sample is placed between the source-sink assemblies as shown in Figure 1. The thermoelectric properties of rutile TiO_2 as well as TiC_xO_{1-x} were studied. A constant input power is applied and the corresponding rise in temperature ΔT_S and voltage developed across the sample ΔE is measured. The Seebeck coefficient **S** can then be calculated using the equation

$$S = \Delta E / \Delta T_S$$

Figure 9 shows the variation of Seekback coefficient with temperature according to the proposed reaction. It was found that the Seebeck coefficient of rutile is negative, suggesting n type carriers, and can be very large at low temperature due to phonon-drag effect. Its magnitude decreases and saturates between 500-1000 μV/K near room temperature.

The thermal conductivity of bulk rutile falls in the range of 5-10 W/Km at room temperature. The Seek back coefficient changes with the reaction of TiO_2 and graphite, because at each and every steps of synthesis different type of TiC_xO_{1-x} is formed. At the last moment TiC is formed at 1500^{o}C. From TiO_2 to TiC, different types of semiconducting compound are formed by the reduction of TiO_2 with graphite. It is evident from the Figure 9 that the Seekback coefficients first decrease with increase the temperature. At this moment only TiO_2 is active. But with increase the temperature beyond 800^{o}C, it was found that the Seeback coefficient was found to change from negative to slight positive. The Introducing oxygen vacancy decreases both the thermal conductivity and Seebeck coefficient in $TiO_{2-\delta}$ [16-18]. At the same time the electrical resistivity decreases drastically due to the increase in the carrier concentration in the reduced samples.

Conclusion

1. TiC_xO_{1-x}/ TiO_2 nano-ceramic was synthesized from SPS technique. TiC_xO_{1-x} are uniformly dispersed in TiO_2 matrix, investigated from SEM examination.
2. Maximum shrinkage occurs at the higher temperature.
3. TiC_xO_{1-x}/ TiO_2 nanocomposite with full density is obtained using the SPS route at relative higher sintering temperature. At the higher temperature maximum TiO_2 tried to convert into TiC_xO_{1-x} and non- stoichiometric TiC_xO_{1-x} react with graphite and the maximum amount of TiC is formed. SPS route clear superiority in terms of achieving faster densification of TiC_xO_{1-x}/TiO_2 composites at the higher temperature. This information has got from the XRD investigation.
4. Remarkable high hardness of 25-28 GPa is achieved in dense SPS-processed TiC_xO_{1-x}/TiO_2 composite. The dense microstructure containing submicron TiO_2 matrix and different types of nano TiC_xO_{1-x} reinforcement is observed to be responsible for the high hardness, formed due to carbothremal reaction. This has also been observed in thermal conductivity.
5. The nature of composite material was studied by Seeback effect. Carbothermal reaction between TiO_2 and graphite is responsible for changing the n-type carrier in TiO_2 to p-type carrier in TiC_xO_{1-x}.

Reference

[1] B Basu, J H Lee and D Y Kim "Processing of Nanoceramic and Nanocompostes : New Result" Key Engineering Vols. 264-268(2004) pp2293-2296.

[2] N Zarrinfar, P H Shipway, A R Kennedy and, A Saidi "Carbide stoichiometry in TiC_x and Cu–TiCx produced by self-propagating high-temperature synthesis" Scripta Materialia 46 (2002) 121–126

[3] R D Shull: Nano Structured Materials 2 (1993) p. 213.

[4] R S Averbek, H J Holfer, and R Tao: Materials Science and Engineering A66 (1993) p. 169.

[5] S Komarneni: J. Mater. Chem., 2 [12] (1992) p.1219.

[6] C Suryanarayana: International Materials Reviews, 40 (1995) p.41.

[7] Young Il Lee, Jong-Heun Lee*, Seong-Hyeon Hong, Doh-Yeon Kim "Preparation of nanostructured TiO_2 ceramics by spark plasma sintering" Materials Research Bulletin 38 (2003) 925–930

[8] Guo-Dong Zhan and Amiya Mukherjee "Processing and characterization of Nanoceramic composite with interesting structural and Functional Properties" Rev.Adv. Mater.Sci.10 (2005)185-196

[9]M T Swihart, Vapor-phase Synthesis of Nanoparticles, *Current Opinion in Colloid and* Interface Science, **8**, 127-133(2003).

[10] Z Shen, M Johnsson, Z Zhao, and M Nygren, Spark Plasma Sintering of Alumina, *J. Am. Ceram. Soc.*, **85**, 1921-27 (2002).

[11] S Tekeli, M Erdogan, and B Aktas, Microstructural Evolution in 8 mol% Y2O3-Stabilized Cubic Zirconia (8YSCZ) with SiO_2 Addition, *Mater. Sci. Eng. A***386**, 1-9 (2004).

[12] Yang Yu-xing, QI Rui. X-ray diffraction analysis [M]. Shanghai: Shanghai Jiao-tong University Press, 1994: 129. (in Chinese)

[13] Li Shu-tang. Base of crystallology about X-ray diffraction [M]. Beijing: Metallurgical Industry Press, 1990: 154−155. (in Chinese)

[14] M Razavi, M R Rahimipour , R Kaboli . Synthesis of TiC nanocomposite powder from impure TiO_2 and carbon black by mechanically activated sintering [J]. Journal of Alloys and Compounds, 2008, 460(1/2): 694−698.

[15] B H Lohse, A Calka, D Wexler. Effect of starting composition on the synthesis of nanocrystalline TiC during milling of titanium and carbon [J]. Journal of Alloys and Compounds, 2005, 394(1/2): 148−151.

[16] F A Grant, *Properties of Rutile (Titanium Dioxide).* Reviews of Modern Physics, **31**(3) 646 (1959).

[17] W R Thurber and A J H Mante, Phys. Rev., **139**, A 1655 (1965).

[18] B I Boltaks, F I Vasenin, and A E Salunina, Zhurnal Tekhnicheskoi Fiziki, **21**(5) 532 (1951)

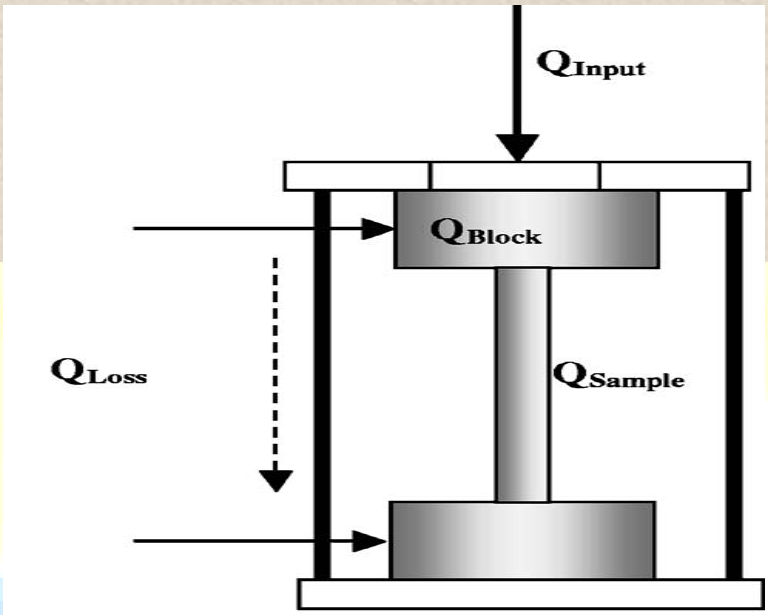

Figure 1. Schematic diagram of the different heat-flow with sample.

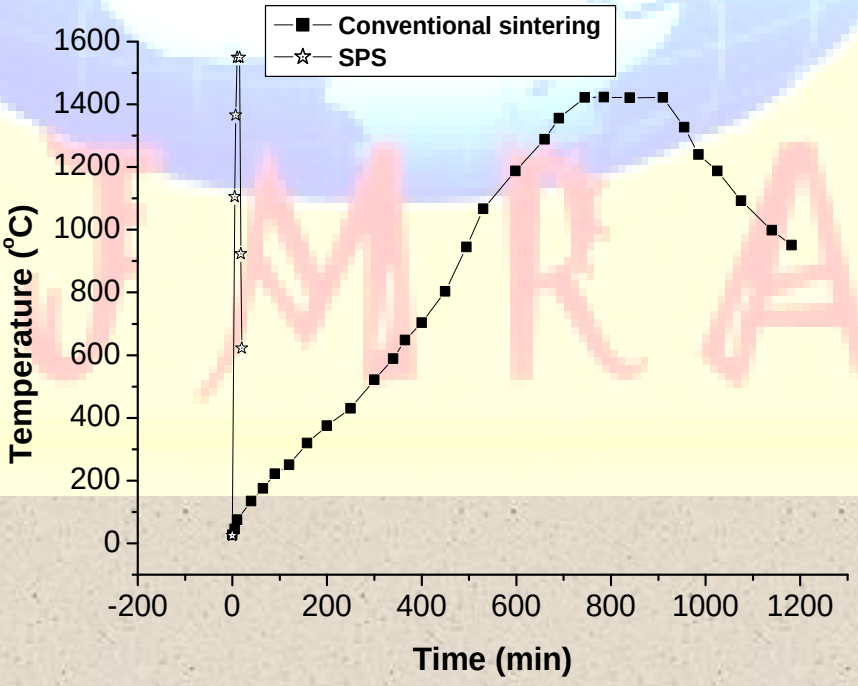

Figure 2. Comparison of sintering profiles of ceramics obtained by conventional sintering and by SPS.

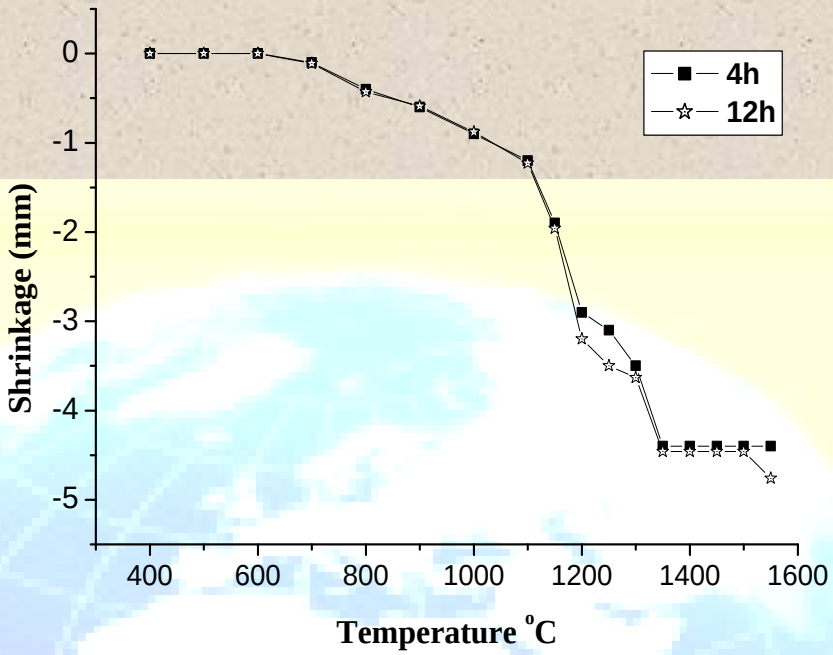

Figure 3. Shrinkage of the powder during sintering

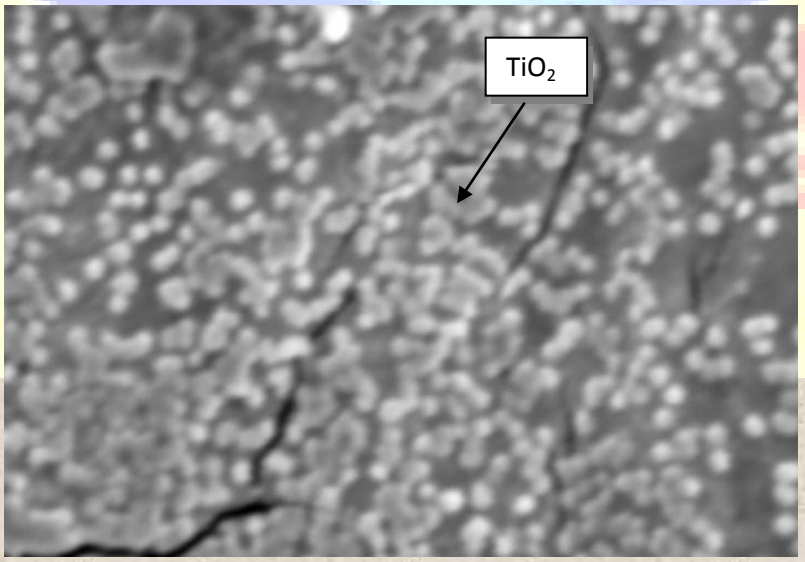

Figure 4.SEM micrograph of TiO_2 nanoparticle

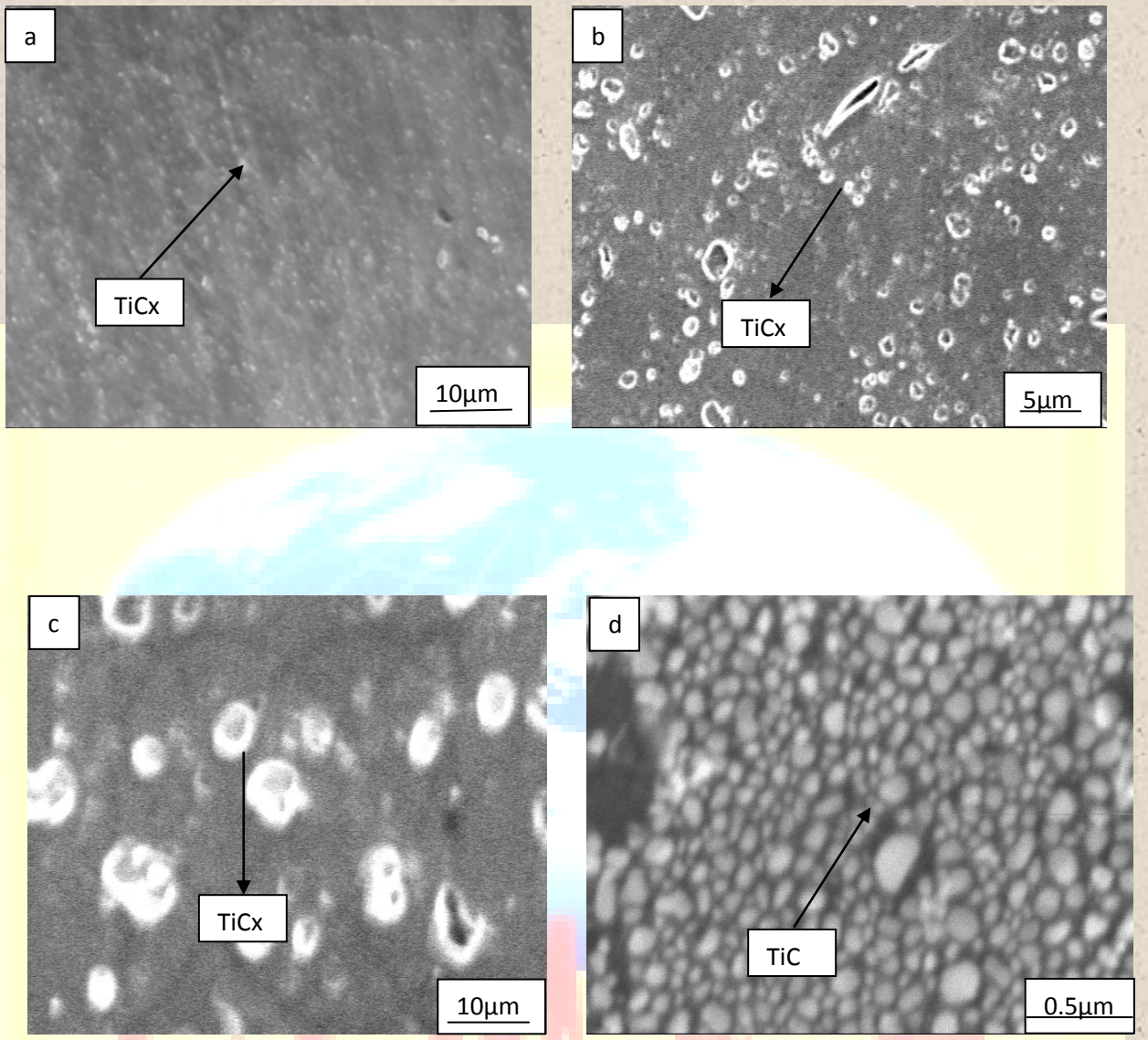

Figure 5. SEM Microgarph of TiC formed at the different temperature (a) 1200 (b) 1300 (c) 1400 and (d) 1500°C

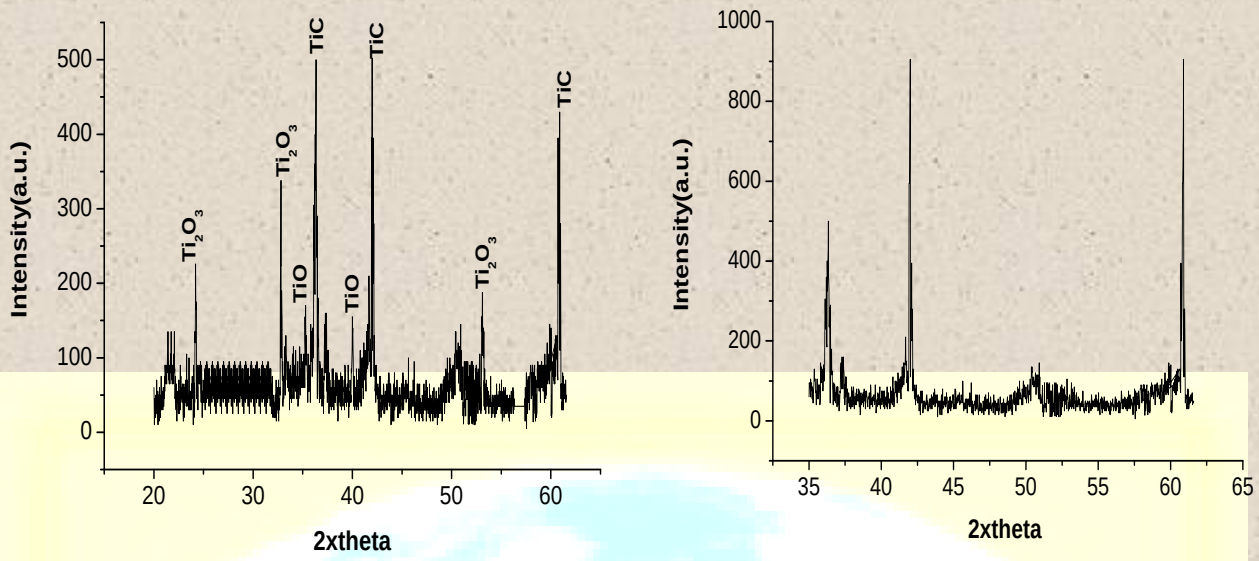

Figure 6. XRD pattern of ultrafine TiC powders prepared at (a) 1300(b) 1550 °C for 4 h

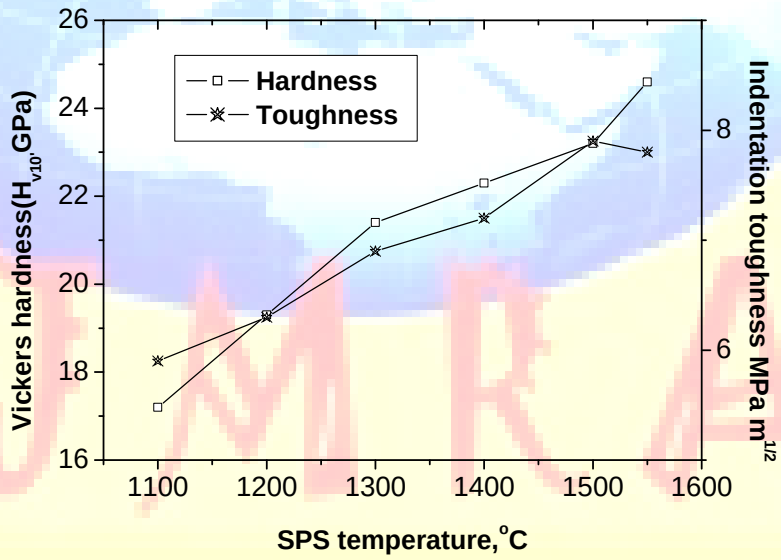

Figure 7. Effect of temperature on density and grain size of conventionally sintered TiO_2 nanoceramics.

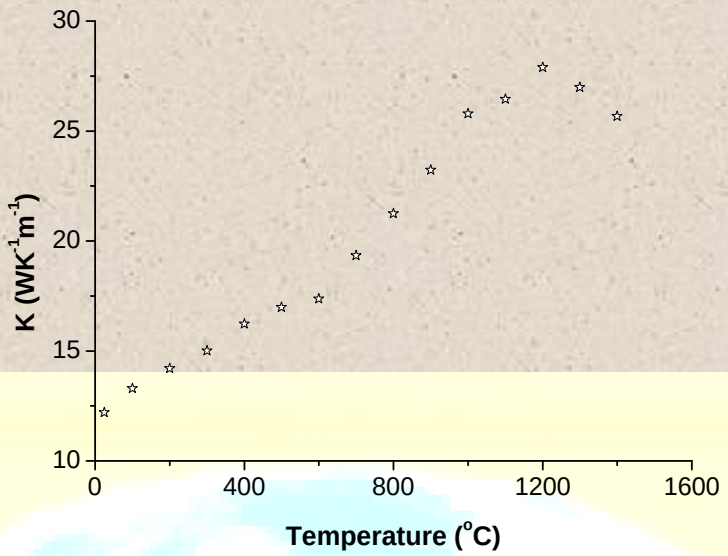

Figure 8. Thermal conductivity of TiO_2/ TiC_xO_{1-x} Nano- Composite as a function of temperature.

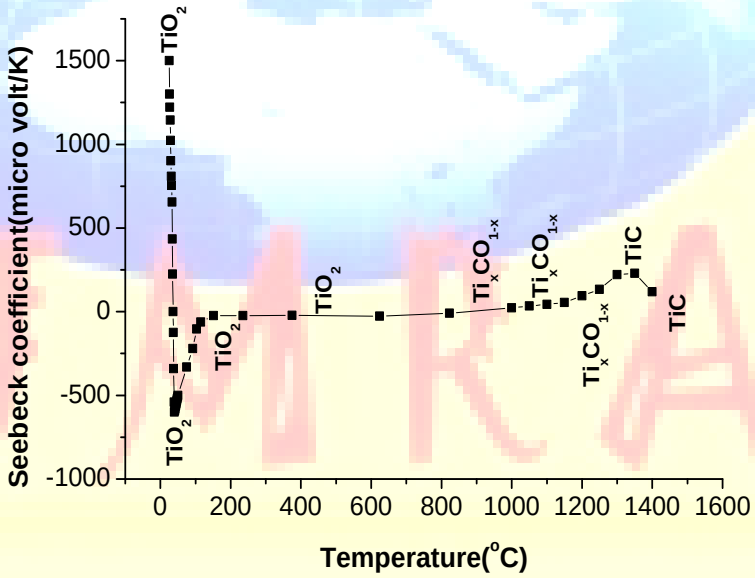

Figure 9. Seeback coefficient of TiO_2/ TiC_xO_{1-x} Nano- Composite as a function of temperature.